Applied Thermal Engineering 226 (2023) 120311

Contents lists available at ScienceDirect

Applied Thermal Engineering

journal homepage: www.elsevier.com/locate/apthermeng

Research Paper

Evaluating the proficiency of a novel solar evacuated tube collector

Xingxing Yang [a,b,c], Qing Lin [a,b,*], Pavitra Singh [d], Fahid Riaz [e], Manoj Kumar Agrawal [f], Theyab R. Alsenani [g], Guangqiang Li Xia [h,*], Mostafa A.H. Abdelmohimen [i,j]

[a] College of Biomedical Information and Engineering, Hainan Medical University, Haikou 571199, China
[b] Guangxi Key Laboratory of Nuclear Physics and Nuclear Technology, Guangxi Normal University,Guilin 541004, China
[c] Department of Civil Engineering, Jiangxi Water Resources Institute, Nanchang 330013, China
[d] Department of Mechanical Engineering, National Institute of Technology Arunachal Pradesh, India
[e] Mechanical Engineering Department, Abu Dhabi University, Abu Dhabi, P.O. Box 59911, United Arab Emirates
[f] Department of Mechanical Engineering, GLA University Mathura, India
[g] Department of Electrical Engineering, College of Engineering in Al-Kharj, Prince Sattam Bin Abdulaziz University, Al-Kharj 11942, Saudi Arabia
[h] Sustainable Management of Natural Resources and Environment Research Group, Faculty of Environment and Labour Safety, Ton Duc Thang University, Ho Chi Minh City, Viet Nam
[i] Mechanical Engineering Department, College of Engineering, King Khalid University, Abha 61421, Saudi Arabia
[j] Shoubra Faculty of Engineering, Benha University, Cairo 11629, Egypt

ARTICLE INFO

Keywords:
Evacuated tube solar collector
PCM
Porous foam
Nanofluid

ABSTRACT

Evacuated tube collector is a type of solar energy unit that converts solar energy into thermal power; however, the output of this unit is not high. Therefore, the present research attempted to propose a highly efficient unit to transform solar energy into proper forms of energy, including electrical and thermal. In the current numerical study, initially, the overall proficiency of integration of the phase change material in the evacuated tube solar collector is poked and compared with the performance of a maiden renewable-based unit consisting of an evacuated tube collector, photovoltaic module, phase change material, and porous metal foam. Henceforth, by determining the best unit from the overall energy viewpoint, the impact of various factors, including melting temperature of phase change material, nanoparticle mass fraction, and mass flow rate of operating fluid on the operation of the unit, are investigated. According to the obtained results, the evacuated tube collector equipped with the photovoltaic module, phase change material, and porous metal foam has the highest performance among the studied units from the energy viewpoint. The overall performance of the presented unit is calculated to be 13 % higher than the net efficiency of conventional evacuated tube solar collector. It is observed that boosting the mass flow rate of operating fluid from 3.6 to 10.8 L/h enhances the average overall output of the presented unit from 38.55 W to 40.13 W. Reducing the melting point of the phase change material can slightly boost the performance of the unit; according to the simulations, reducing the melting point from 44 °C to 35 °C raises the overall performance of the unit by around 0.4 %. Also, dispersing nanoparticles in the base fluid improves the performance of the unit by 3.3 %.

1. Introduction

Evacuated tube collector (ETC) is a typical solar energy unit that transforms solar energy to heat to maintain the buildings' needs or electricity production by using a gas turbine. In this renewable system, solar irradiance absorbs by the absorber layer and terns to the heat. The produced heat in the absorber layer is transferred to the core of the unit and absorbed by the operating fluid.

Combining this solar power unit with Phase Change Materials (PCM) can boost the performance of the unit. The ETC unit provides a considerable amount of heat in the noontime. In contrast, because of the low solar intensity in the morning and afternoon, the solar energy unit's performance is not suitable enough. On the other hand, the PTC unit integrated with PCM (ETC-PCM) has a more consistent performance than the ETC. This is because PCM is a component that can store energy by transfer from solid to liquid phase in high temperatures [1]. This material releases its stored heat to the system at low temperatures [2]. This phenomenon makes the performance systems more reliable. Until now, researchers investigated the application of PCM for heat removal

* Corresponding authors.
E-mail addresses: hy@mailbox.gxnu.edu.cn (Q. Lin), GuangqiangLiXia@gmail.com (G.L. Xia).

https://doi.org/10.1016/j.applthermaleng.2023.120311
Received 23 September 2022; Received in revised form 10 February 2023; Accepted 24 February 2023
Available online 27 February 2023

Nomenclature

A	Area (m^2)
A_{msuh}	Mushy zone coefficient
C_f	Inertial coefficient
C_p	Determined heat capacity at a constant pressure condition ($J/kg \bullet K$)
d	Tube diameter (m)
$\dot{E}$	Energy rate (W)
$\dot{G}$	Solar radiation intensity ($W \bullet m^{-2}$)
g	Gravity ($m \bullet s^{-2}$)
H	Total enthalpy ($J \bullet kg^{-1}$)
K	Permeability
k	Thermal conductivity ($W \bullet m^{-1} \bullet K^{-1}$)
P	Pressure of fluid (kPa)
S	Linear deformation
T	Temperature (K)

Greeks

μ	Fluid dynamic viscosity ($kg/m \bullet s$)
β	The volume fraction of considered liquid
$\varnothing$	Mass fraction of utilized nanofluid
k_B	Boltzmann constant
τ	Transmissivity
η	Efficiency (%)
ρ	Material density (kg/m^3)
σ	Stefan-Boltzmann coefficient ($W/m^2 \bullet K^4$)
ε	Porosity, Emissivity
ϕ	Slight number

Subscripts

amb	Ambient condition
bf	Considered base fluid
cell	PV cell
ele	Electrical energy
g	Glass coating
in	Inlet boundary
loss	Loss
nf	Utilized nanofluid
out	Outlet boundary
r	Standard state
s	Solid-state
sun	Sun
th	Thermal energy
w	Wind effect

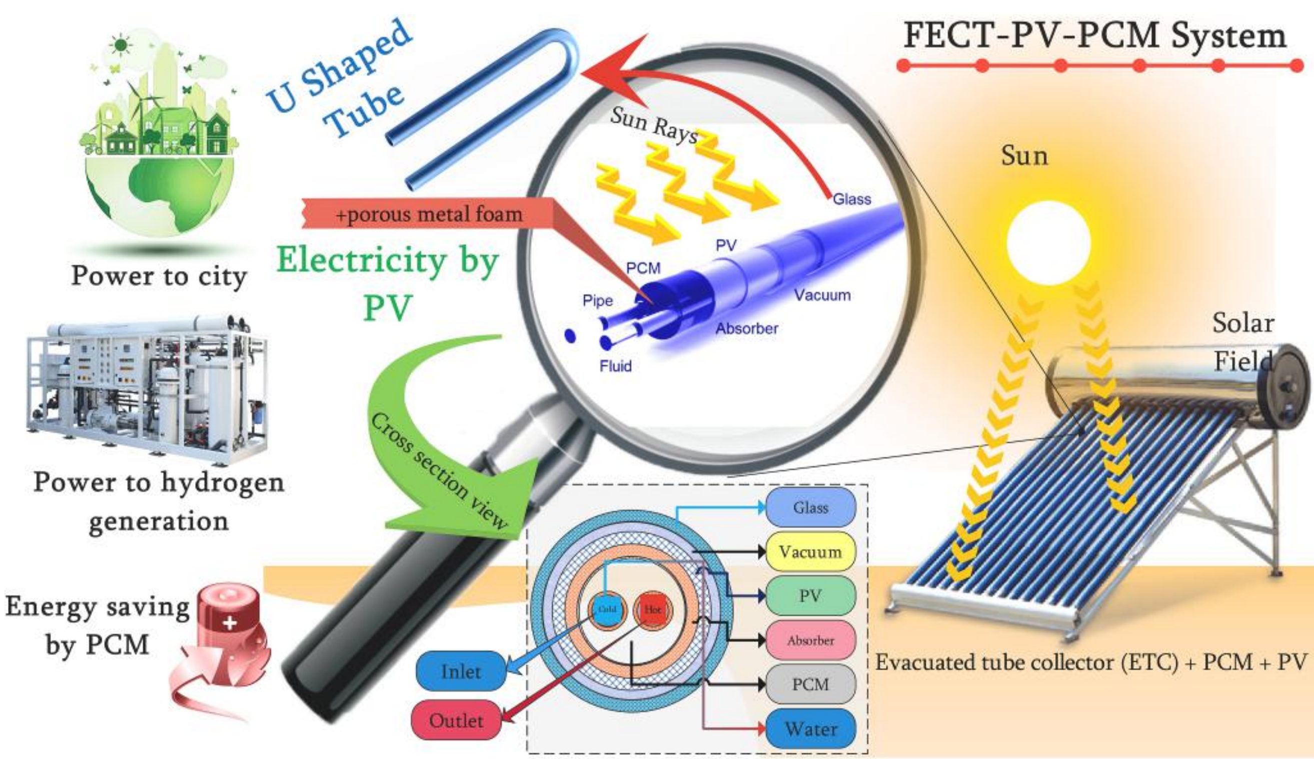

Fig. 1. A 3D face of the FETC-PV-PCM hybrid unit.

[3] and improving the performance of solar power units [4]. In addition, researchers improved the performance of PCM by mixing it with nanoparticles [5,6] or applying a magnetic field [7]. The following explains the experimental and numerical studies on the outputs of the ETC unit integrated with PCM.

For instance, the influence of utilizing PCM on the outputs of an ETC design is scrutinized by Papadimitratos et al. [8], and the impact of considering PCM with various properties on the unit operation is evaluated. It is found that integrating ETC with PCM can remarkably elevate the efficiency of the ETC. Essa et al. [9] poked the effect of the mass flow rate of operating fluid on the outputs of a newfound ETC-PCM generation unit. This study concluded that elevation in the water flow level from 15 L/h (litter per hour) to 21 L/h declined the PCM temperature to around 55 °C. In another study, Chopra et al. [10] scrutinized the

Table 1
Geometrical dimensions of the parts of the FETC-PV-PCM hybrid unit.

Unit component	Dimension (mm)
Outer diameter of the glass	50
Glass thickness	3
Absorber thickness	1
Outer diameter of the pipe	9
Diameter of the fluid media	8
Length of the ETC	1400

Table 2
Thermal properties of the parts of the solar energy units [28,29].

Parts	Density ($kg \bullet m^{-3}$)	Thermal conductivity coefficient ($W \bullet m^{-1} \bullet K^{-1}$)	Specific heat at a fixed pressure ($J \bullet kg^{-1} \bullet K^{-1}$)
Glass coating	2200	0.76	830
PV cell	2330	148	700
Absorber, pipe, and foam	8960	401	385

Table 3
The MWCNT/water nanofluid properties in the single-phase model [31–33].

Unit component	Property	Eq. number
Density	$\rho_{nf} = (1-\phi)\rho_{bf} + \phi\rho_{nf}$	(1)
Heat capacity	$C_{p,nf} = (1-\phi)C_{p,bf} + \phi C_{p,nf}$	(2)
Thermal conductivity	$k_{nf} = \left[\frac{k_p + 2k_{bf} - 2\phi(k_{bf}-k_p)}{k_p + 2k_{bf} + \phi(k_{bf}-k_p)} + \frac{\rho_p\phi C_{p,bf}}{2k_{bf}} \bullet \sqrt{\frac{2\kappa_B T}{3\pi d_p \mu_{bf}}}\right] k_{bf}$	(3)
Viscosity	$\mu_{nf} = \frac{\mu_{bf}}{1 - 34.87\left(\frac{d_p}{d_{bf}}\right)^{-0.3}\phi^{1.03}}\mu_{bf}$	(4)

Table 4
Balance equations of solid, PCM, and water sections of the hybrid unit [34,35].

Explanation	Balance equation	Eq. number
	Water	
Continuity	$\frac{\partial\rho_f}{\partial t} + \nabla \bullet \left(\rho_f \vec{V}_f\right) = 0$	(5)
Momentum	$\frac{\rho_f}{\varepsilon}\left(\frac{\partial\vec{V}_f}{\partial t} + \frac{1}{\varepsilon}\vec{V}_f \bullet \nabla\vec{V}_f\right) = -\nabla P + \frac{\mu_f}{\varepsilon}\nabla^2\vec{V}_f - \rho_f g - \left(\frac{\mu_f}{K} - \frac{\rho_f C_f\lvert V_f\rvert}{\sqrt{K}}\right)V_f$	(6)
Energy	$\left[\varepsilon(\rho C_p)_f + (1-\varepsilon)(\rho C_p)_{foam}\right]\frac{\partial T}{\partial t} + (\rho C_p)_f(V_f \bullet \nabla T) = k_e\nabla^2 T$	(7)
	Solid	
Energy	$\rho C_{p,s}\frac{\partial T}{\partial t} = \nabla \bullet (k_f\nabla T)$	(8)
	PCM	
Mass	$\frac{\partial p}{\partial t} = -\nabla \bullet \left(p \bullet \vec{V}\right)$	(9)
Momentum	$-p\left[-\frac{\partial\vec{V}}{\partial t} - \left(\vec{V} \bullet \nabla\right)\vec{V}\right] + \nabla P - \nabla \bullet \left(\mu\nabla\vec{V}\right) - S = 0$	(10)
S function	$S = \frac{(1-\beta)^2}{(\beta + \varnothing)}A_{mush}\left(\vec{V} - \vec{V}_p\right)$	(11)
Energy	$\frac{\partial}{\partial t}(pH) + \nabla \bullet \left(p\vec{V}H\right) = \nabla \bullet (k\nabla T) + S$	(12)
Enthalpy	$H = h_{ref} + \int_{T_{ref}}^{T} C_{p,PCM}dT + \beta L$	(13)
Liquid fraction	$\beta = \begin{cases} 0 if T < T_{melting} \\ 1 if T > T_{melting} \end{cases}$	(14)

Table 5
The operating conditions of the base case.

Parameter	Base case quantity	Bound
Melting spot (°C)	40	35–44
Specific enthalpy ($kJ \bullet kg^{-1}$)	160	–
Conductivity ($W \bullet m^{-1} \bullet K^{-1}$)	0.2	–
Inlet mass flow rate ($L \bullet h^{-1}$)	7.2	3.6–10.8
Nanofluid mass fraction (%)	0	0–4 %

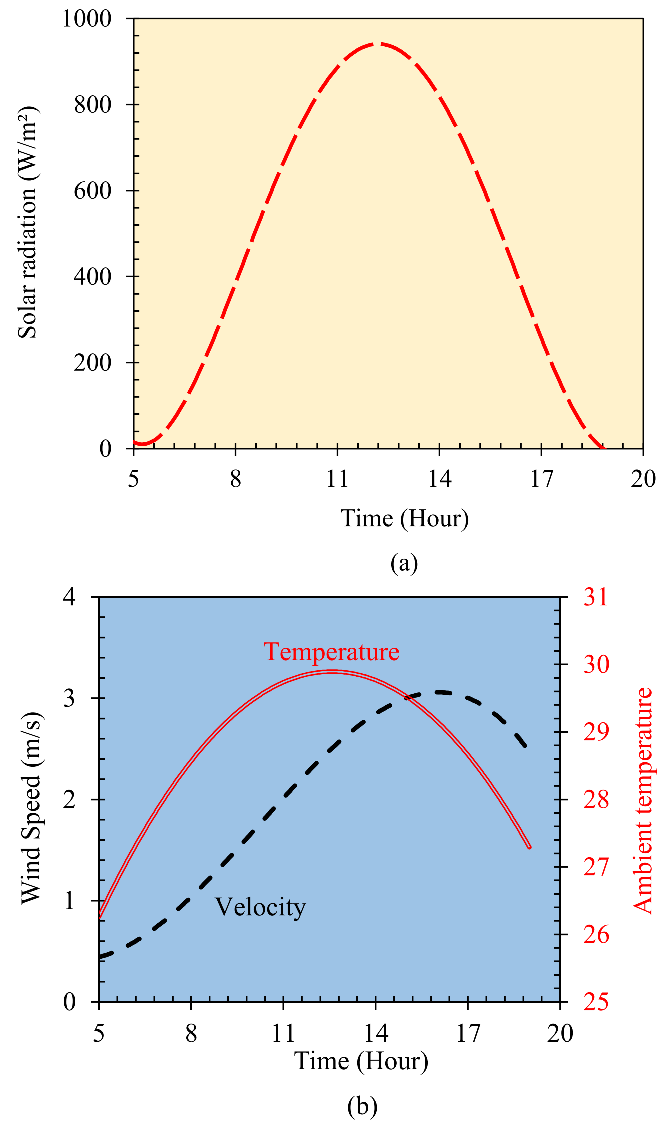

Fig. 2. Changing the (a) DNI and (b) ambient temperature and wind velocity during the simulated day.

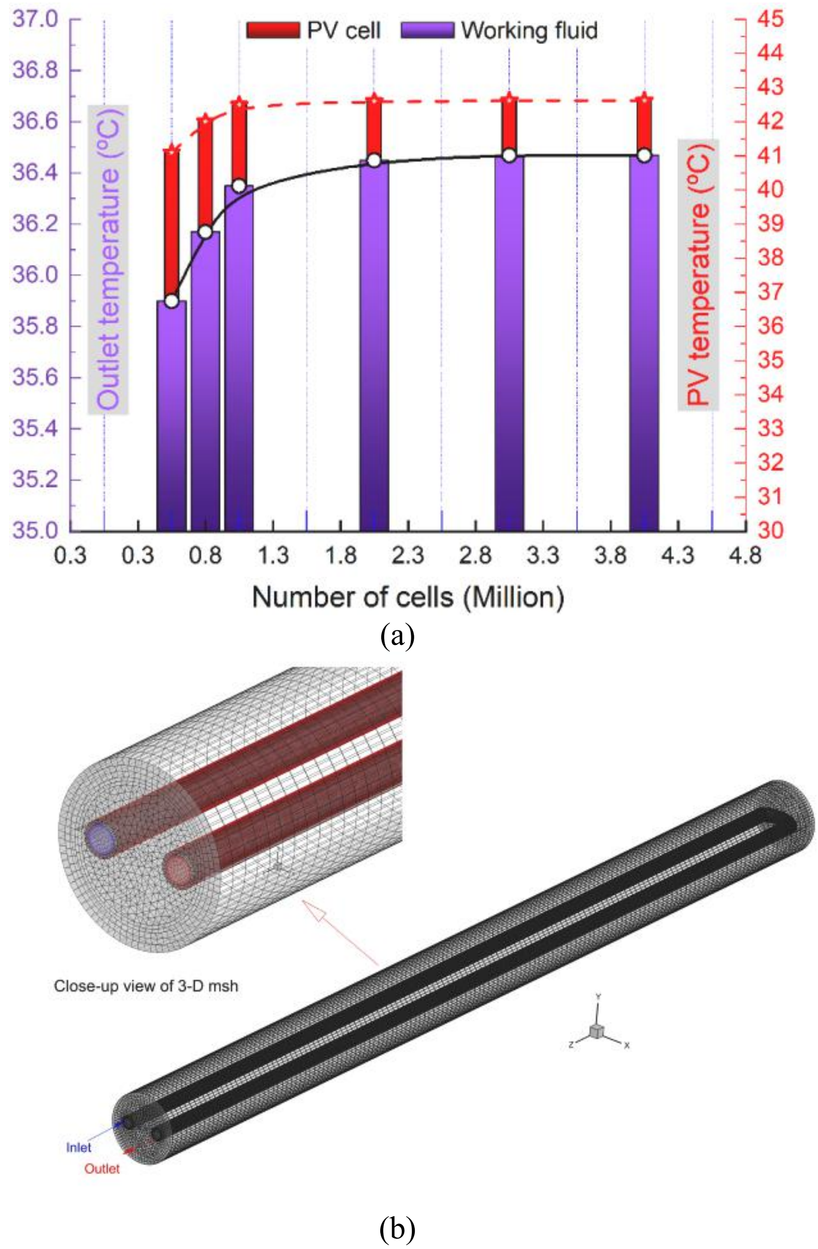

Fig. 3. (a) The variation of outlet temperature and PV layer temperature versus the number of cells. (b) A 3-D view of the generated mesh.

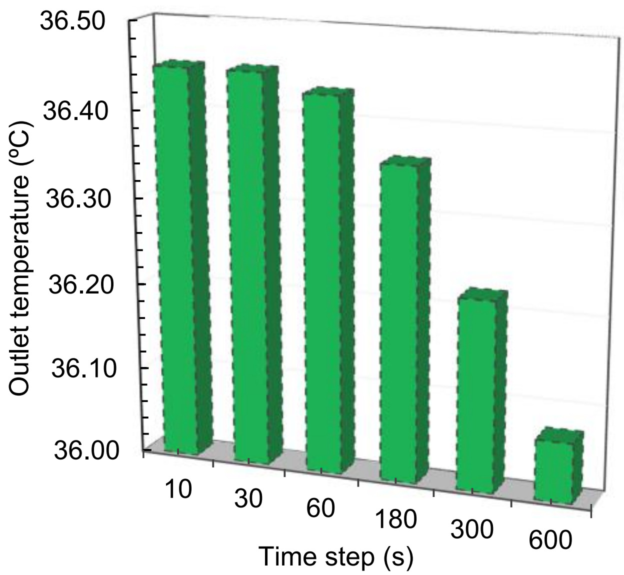

Fig. 4. The outlet temperature of the operating fluid versus time step size.

performance of an ETC unit integrated with heat pipe and PCM. In this study, it is revealed that using PCM in the ETC unit prevents the overheating problem.

Additionally, the effect of the installation of aluminum fins in the PCM-based ETC unit is investigated by Abokersh et al. [11]. This study concluded that using fins reduces the thermal performance of the unit by around 14 % during the day while it enhances the working duration of the unit after sunset. The comparison between the performance of a heat pipe-based ETC without/with combining by PCM is performed by Chopra et al. [12]. According to their outcomes, the energy performance of mentioned heat pipe-based ETC unit integrated with PCM is around 33 % and 38 % higher than that of the unit without PCM in the operating fluid mass flow rates of 1200 L/h and 300 L/h, respectively.

In a recent research on the ETC-PCM unit, Olfian et al. [13] examined the influence of using a corrugated tube in the unit to enhance the outputs of the unit. Based on the results of this investigation, the thermal output of the PCM-based ETC unit with a smooth tube is 22 % less than the unit thermal output with a corrugated tube. Essa et al. [14] evaluated the impact of heat pipes with helical finned on the output of an ETC-PCM unit. This research found that the overall efficiency of the unit with helical fins is more than that of conventional ones. Furthermore, they observed that using helical fins delays the melting process of PCM in the unit, which benefit the output power of the unit. The impact of PCM characteristics, such as enthalpy, thermal conductivity, and melting point on the thermal performance of an ETC unit, is studied by Feng et al. [15]. Based on this study, reducing the PCM melting point improves the thermal power of the unit. Also, the PCM with an enthalpy of 170 kJ/kg had the highest positive influence on the performance of the unit.

Based on these studies, integrating the ETC unit with the PCM can enhance the performance of the unit due to its energy storage in the noontime and thermal energy released in periods with low solar radiation intensity.

Also another method that can elevate the performance of solar power units is nanoparticle fusion to the operating fluid [16]. According to the research, adding nanoparticles to the base fluid improves the operating fluid thermal characteristics [17], which can intensify the fluid heat transfer rate within the channel as well as ascend the performance of

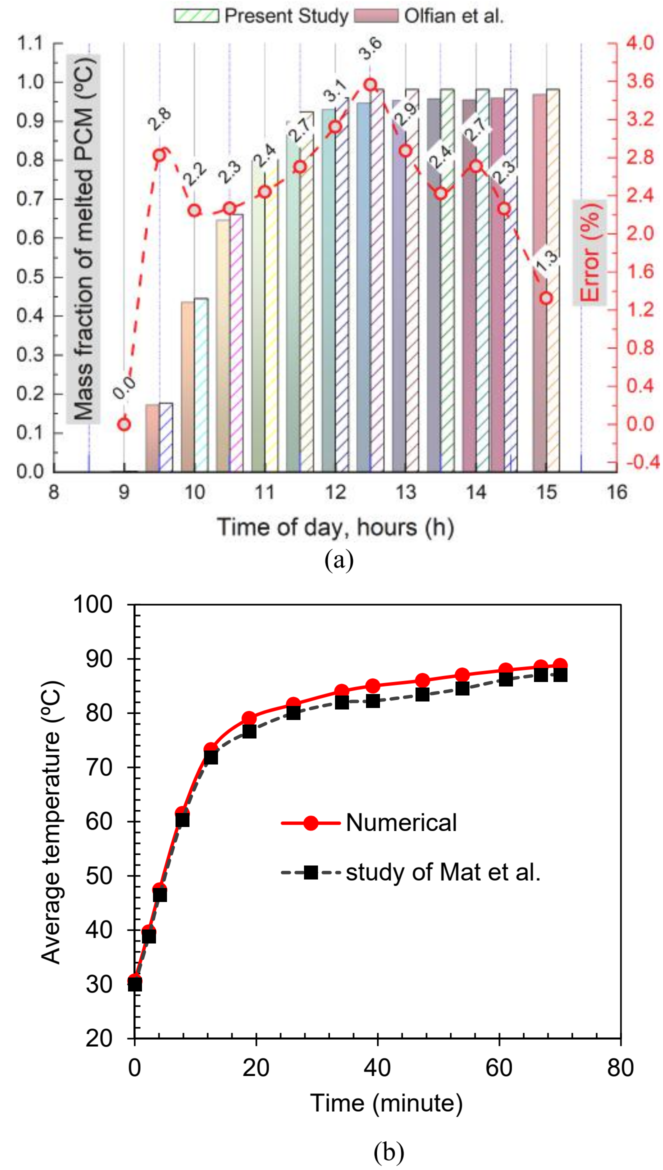

Fig. 5. (a) Comparison between the amount of melted PCM in the present investigation and the assessment of Olfian et al. [13], and (b) comparison between the amount of average temperature of PCM in the evaluation of Mat et al. and present perusal [44].

solar energy units, including ETC [18–20].

Kaya et al. [21] experimentally evaluated the effect of using pure water, Cu_2O/water (4 %), and Cu_2O/water (8 %) as the operating fluid of the ETC-PCM unit. The outputs of this study show that the unit using Cu_2O/water (8 % vol.) nanofluid has energy and exergy efficiency of around 60 % and 6 %, respectively, which is the highest performance among the studied units. In another experimental study, Hosseini and Dehaj [22] examined the effect of adding TiO_2 Nanoparticles (NP) and Nanowires (NW) in the base fluid of the ETC unit. These experimental tests reveal that using TiO_2 NWs-nanofluid can enhance the performance of the ETC unit by approximately 21 %. Moreover, in a numerical investigation, Kaya et al. [21] assessed the performance of the Al_2O_3/water-based ETC unit. The numerical outputs of this investigation show that the unit with bricks-shaped Al_2O_3/water nanofluids has the highest

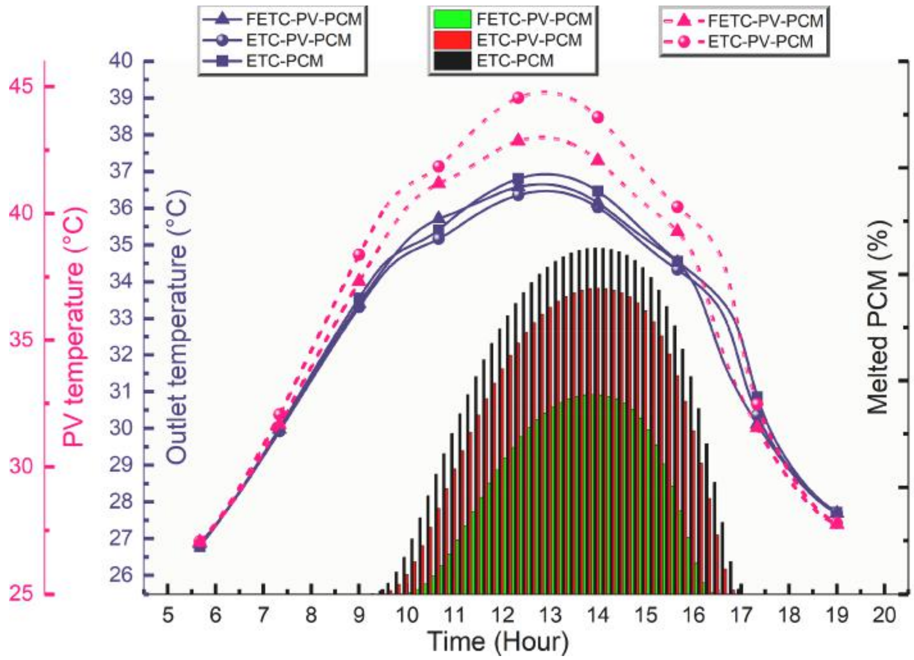

Fig. 6. The outlet temperature, PV layer temperature, and melted PCM for different units at the base case.

performance.

As mentioned above, even though the integration of the ETC unit with the PCM and nanofluids can enhance the thermal performance of the unit, the overall efficiency of the unit is not high enough. Integrating the ETC unit with the Photovoltaic (PV) module can properly increase ETC unit performance. Using a PV cell as the absorber of the unit can lead to the production of both thermal and electrical energy by the unit simultaneously. However, it should be noted that the PV cell operation is highly dependent on the cell's temperature [23]. Increasing the PV cells temperature declines their performances remarkably [24].

Moreover, installing metal foams in the fluid channel of the ETC unit may enhance the total performance of the unit. The metal foam has a high thermal conductivity which can intensify the rate of heat transfer through the unit. This material can be used inside the fluid channels to enhance the transferred heat to the operating fluid or inside the PCM media to improve its extremely low thermal conductivity [25–27].

In the current research, the overall performance of a PCM-based ETC unit is compared with the output of an ETC-PCM unit combined with a PV cell module (ETC-PV-PCM) and an ETC-PV-PCM unit that its fluid channel filled with a porous metal foam (FETC-PV-PCM). Filling the fluid channel with the porous metal foam raises the contraction between the fluid and the pipe wall, which causes an improvement in the operating fluid heat transmit rate. Henceforth, by detecting the unit with the highest performance, the impacts of different factors, including fluid mass flow rate, the PCM melting state, and mass fraction of nanoparticles on the efficiency of the chosen unit, are poked. Furthermore, all simulation procedures are performed using the transient approach with variable ambient temperature, wind speed, solar intensity, and sky temperature.

2. Numerical model

In the current research, the effect of combining an ETC unit with various components such as PCM, porous metal foam, and PV module is studied to propose a unit with the highest performance. In the first step, the efficiency of the mentioned units is collated with the base case condition. Henceforth the impact of different parameters on the efficiency of the best unit is evaluated. In Fig. 1, a 3D view of the FETC-PV-PCM is presented. This figure shows that the FETC-PV-PCM hybrid unit consists of a glass cover, a vacuumed media, a PV module layer, a copper layer, PCM, and a copper pipe filled with porous metal foam. The difference between this unit and the ETC-PV-PCM hybrid unit is lacking porous metal foam in the fluid channel. Also, the ETC-PCM unit does not have both the PV layer and porous metal foam.

In the FETC-PV-PCM hybrid unit, the solar intensity absorbs in the PV layer. In this layer, a part of solar radiation converts to electrical energy directly. While the rest of solar radiation converts to heat. The produced heat in the absorber layer is transferred to both the environment and the core of the unit. A part of the thermal energy transfers to the ambient through the radiation mechanism to the sky. The rest will deliver to the operating fluid through conduction and convection heat transfer. The geometrical dimensions of some parts of the FETC-PV-PCM hybrid unit are listed in Table 1. Also, the properties of the components of the units are provided in Table 2.

As mentioned earlier, the impact of nanoparticle dispersion in pure water is examined to enhance the ETC unit's performance. In this study, the MWCNT nanoparticles are mixed with the base fluid to boost the unit's overall efficiency. The specific heat capacity, density, and thermal conductivity of MWCNT nanoparticles are 3000 $W \bullet m^{-1} \bullet K^{-1}$, 1600 $kg \bullet m^{-3}$, and 769 $J \bullet kg^{-1} \bullet K^{-1}$, respectively [30]. In the present simulations, the single-phase model is used to apply the effect of fusing nanoparticles in pure water. In this approach, the mixture's heat capacity, density, thermal conductivity, and viscosity can be calculated as presented in Table 3 [31–33].

In these equations, T, k, μ, ρ, and C_p refer to the temperature, thermal conductivity, viscosity, density, and specific heat capacity, respectively. Moreover, d and ϕ donate the diameter and mass fraction, respectively.

3. Equations and numerical details

The current section explains the governing equations of the units, numerical assumptions, and boundary conditions of the units.

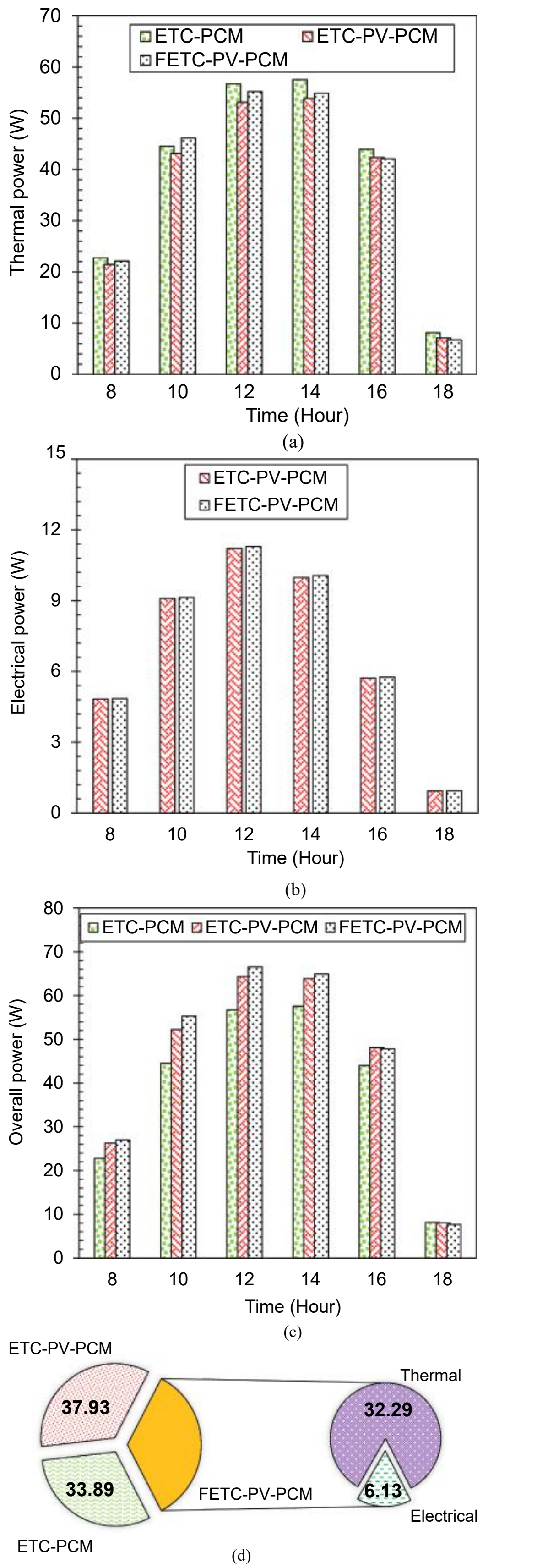

Fig. 7. (a) Thermal output, (b) electrical output, (c) overall output, and (d) average power of the hybrid units during the day at the conditions of the base case.

3.1. Governing equations

By choosing the ETC units as a control volume, balance equations for water, PCM, and solid components can be written as pictured in Table 4.

In the equations presented in Table 4, H, β, ϕ, and A_{msuh} refers to the total enthalpy, liquid fraction, slight number (0.001) [36], and mushy zone constant (10^5). The enthalpy-porosity technique is imposed to simulate the PCM in the unit. In this method, the PCM remains in a solid state until getting its melting temperature. At this temperature, the PCM stores thermal energy equal to its latent heat. In storing energy at a constant temperature (melting temperature), the PCM transfers from the solid state to the liquid state. Afterward, by melting all the PCM, its temperature starts to increase again.

Also, in Table 4, K, ε, k_e, and C_f refer to the permeability, porosity, effective conductivity, and inertial coefficient, respectively. For simulating the unit, the amount of permeability and porosity of the copper foam is considered 7×10^{-6} and 0.8, respectively. Moreover, the amount of inertial coefficient and effective conductivity can be obtained as [34,37,38]:

$$C_f = \frac{1.75}{\sqrt{150\varepsilon}\sqrt{\varepsilon}} \tag{15}$$

$$k_e = \varepsilon k_f + (1-\varepsilon)k_{foam} \tag{16}$$

3.2. Thermodynamic analysis

Based on the final and initial energy values of the ETC units, the energy equilibrium of the simulated units can be presented as follows:

$$\dot{E}_{sun} = \dot{E}_{th} + \dot{E}_{ele} + \dot{E}_{loss} \tag{17}$$

here, $\dot{E}_{sun}$ is the solar energy rate absorbed by ETC units, $\dot{E}_{ele}$ is the rate of electrical generation by the ETC-PV-PCM and FETC-PV-PCM renewable units, and $\dot{E}_{loss}$ is the energy loss of the unit. It should be noted that the PCM-based ETC unit cannot supply electrical energy. In Eq. (17), the rate of thermal energy can be presented as follows [39]:

$$\dot{E}_{th} = \dot{m} \bullet C_p \bullet (T_{out} - T_{in}) \tag{18}$$

where, $\dot{m}$ states mass level of water, T_{in} is initial temperature of water, and T_{out} is water outlet temperature. Furthermore, the electrical production of the unit can be calculated as [24,40]:

$$\dot{E}_{ele} = \eta_{pv} \bullet \dot{E}_{sun} \tag{19}$$

$$\dot{E}_{sun} = \dot{G} \bullet A_c \bullet \tau_g \bullet \alpha_{cell} \tag{20}$$

$$\eta_{pv} = \eta_r \bullet [1 - 0.0045 \bullet (T_{cell} - 298.15)] \tag{21}$$

In the above equations, $\dot{G}$, A_c, τ_g, and α_{cell} refer to the solar intensity, absorber area, transmissivity of the glass cover, and PV layer absorptivity, respectively. Additionally, according to Eq. (21), the PV modules electrical efficiency can be estimated based on the standard efficiency (η_r) and PV module temperature (T_{cell}). In this equation, the standard performance of the PV module is considered to be 15 %. Finally, the overall performance of the ETC units can be determined as [41]:

$$\dot{E}_{ov} = \dot{E}_{ele} + \dot{E}_{th} \tag{22}$$

3.3. Boundary conditions

In the numerical models, the “mass flow inlet” boundary conduction is applied at the inlet of the U-shaped channel. The atmospheric pressure is imposed at the tube outlet. Also, for simulating the solar radiation in the units, the “heat generation” situation is considered for the PV layer of the ETC-PV-PCM and FETC-PV-PCM hybrid units are applied. Moreover, in the ETC-PCM renewable unit, the “heat creation” condition is

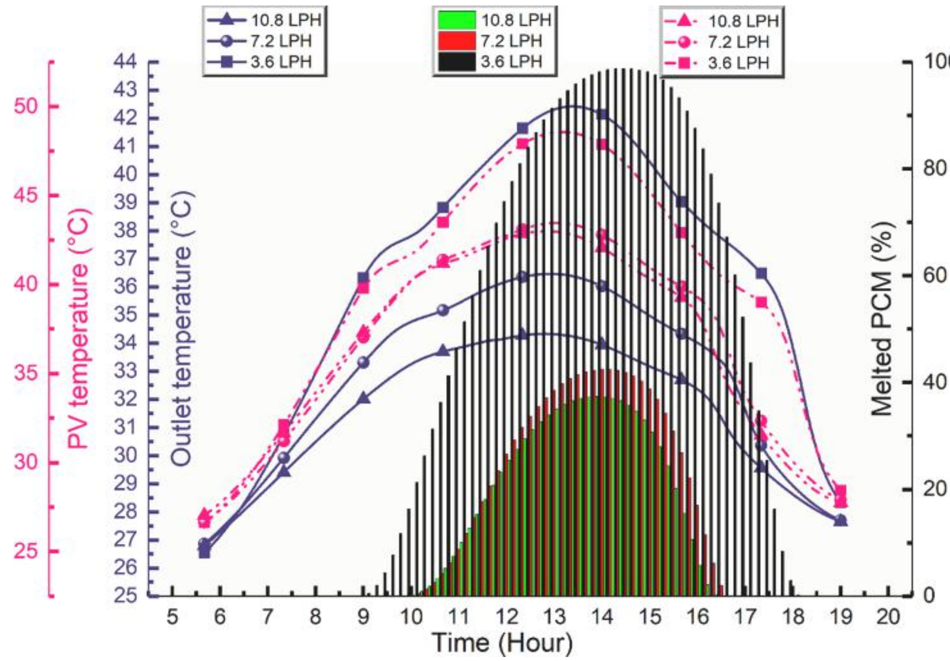

Fig. 8. The melted PCM, PV layer temperature, and outlet temperature of FETC-PV-PCM unit at different water mass flow rates.

implemented in the absorber layer. In the current study, the modeling of the units is done at the base case condition. Also, for evaluating the effect of various parameters, every time, one parameter is variable (the target parameter), and the other parameters are equal to the operating conditions of the base case. The range of studied factors and base case conditions are presented in Table 5.

Besides, for the convection and radiation heat transfer simulation from the unit to the ambient, the outer surface of the unit is considered "wall" with "mixed heat transfer" condition. To simulate the convection and radiation heat transfer mechanisms, the sky temperature and convective heat transfer coefficient are calculated as [42,43]:

$$h_w = V_w^{0.58} d_g^{-0.42} \tag{23}$$

$$T_{sky} = 0.0522 T_{amb}^{1.5} \tag{24}$$

As presented in Eq. (23) and (24), the convective heat transfer coefficient depends on collector diameter and wind speed. Furthermore, the sky temperature is the function of ambient temperature. For the modeling of the units, the ambient temperature, solar radiation, and wind speed are varied during the time presented in Fig. 2. It should be noted that, in these simulations, the amount of water inlet temperature and the ambient temperature is considered to be equal.

In the present study, for simplifications in the simulations, the following assumptions are made:

- The surface of the glass coating is considered to be clean without any external obstacles on its surface.
- The properties of all the unit components, including PCM, are considered constant with variations in the unit's temperature.
- The single-phase model is used to study the impact of nanoparticles dispersion in the water
- The sky is supposed to be a black body.

4. Mesh study and validation

In this section of the present paper, the influence of the mesh distribution and time step size on the output results of the simulation and the validity of the numerical results are discussed. Fig. 3 presents the variation of outlet and PV layer temperature versus the number of cells. The FETC-PV-PCM unit meshed with 500, 750, 1000, 2000, and 4000 thousand cells to study the impact of mesh quality on the results. The results of the mesh study show that an increase in the number of PV cells from 500 to 1000 raises both outlet and PV temperature rapidly. While by elevation of cell numbers from 1000 to 4000 thousand cells, just a minor variation in the numerical outputs can be seen. According to the numerical results, the unit with 2000 cells is chosen for the following simulation, pictured in Fig. 3 (b). As indicated, all unit components except PCM have meshed with hexahedron cells. Due to the complexity of the PCM media, this part of the unit meshed with tetrahedron cells. Also, some thin layers are created in the operating fluid volume near the tube wall to capture the temperature and velocity gradients of the fluid accurately. The same mesh density is employed for both ETC-PCM and ETC-PV-PCM units.

In addition to the independency of obtained results from the number of cells, the numerical outputs should be independent of the time step size in the numerical simulations. Therefore, the effect of this critical parameter on the simulations is investigated. In Fig. 4, the effect of time size on the operating fluid outlet temperature is outlined. As presented in this figure, in the large time steps, such as 600 s and 300 s, the obtained results are not reliable due to their sensitivity to the variation of time step size. By reducing the time step size from 600 s to 300 s and from 300 s to 180 s, the variation in the outlet temperatures of the operating fluid is 0.15 °C and 0.14 °C, respectively.

On the other hand, a reduction in the time step size from 60 s to 30 s and 10 s has a minor effect on the unit's performance. Therefore, to simulate the designed units, the time step size is considered 30 s. It is noteworthy to mention that the presented results for both mesh and time

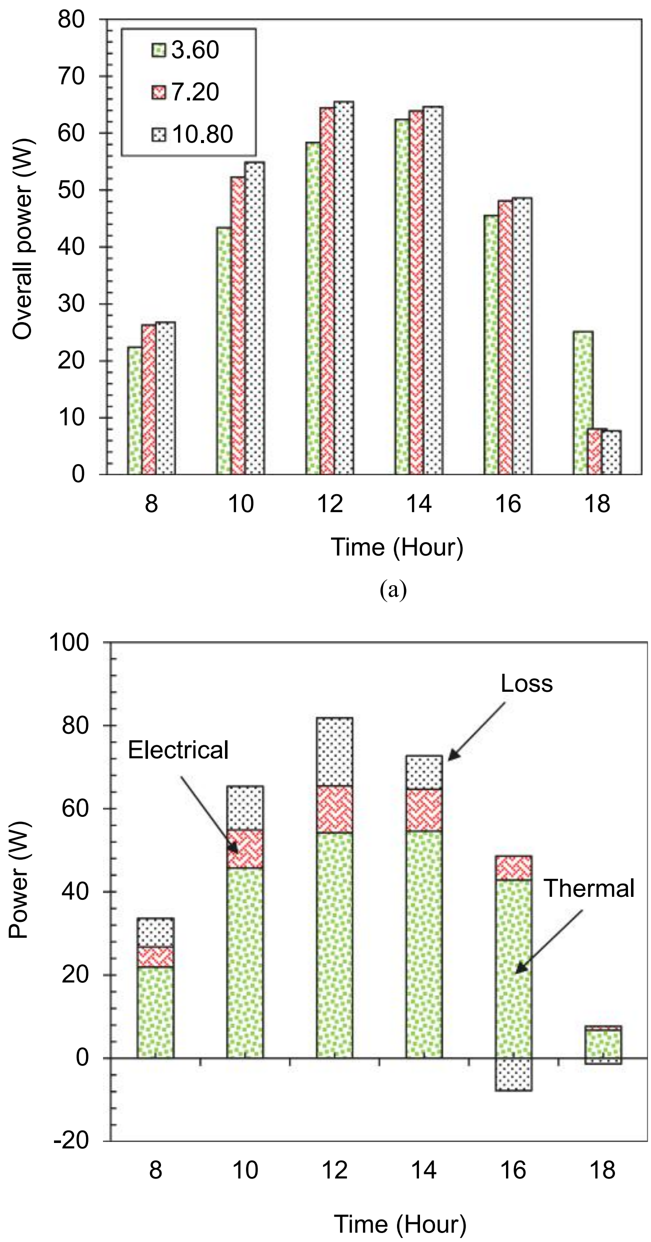

(a)

(b)

Fig. 9. (a) The overall performance of different units by variation of water mass flow rates and (b) the detailed performance of the unit at the water flow level of 10.8 L/h.

step size independency belong to the FETC-PV-PCM unit at the noontime.

In addition, for the validity of the numerical outputs, the present study results are compared with the numerical results of Olfian et al. [13]. To compare the current data with the obtained information from Olfian et al. [13], the specification of the present study is chosen as the reference mentioned. In this order, the inner glass tube dimensions, outer glass tube, U-shaped tube diameter, and collector length are assumed to be 37 mm, 47 mm, 6 mm, and 500 mm, respectively. Moreover, the inlet temperature and velocity of the fluid are 30 °C and 0.04 m/s, respectively.

The achieved outcomes of the current appraisal and the evaluation of Olfian et al. [13] are evoked in Fig. 5. As time elapsed, the melted PCM mass fraction rose gradually, which can be attributed to the increased solar intensity from the morning until noon. Based on the results, there is a minor difference between the studies. The maximum and average errors between the studies are 3.7 % and 2.4 %, respectively. As a result, the numerical results of the present study are in excellent agreement with the results of the investigation of Olfian et al. [13].

On top of that, to investigate the validity of the outputs, the numerical outcomes are compared with the data of Mat et al. [44]. In the mentioned study, the melting phenomenon of PCM in a smooth tube is evaluated. The dimensions of the designed geometry are considered the same as the experimental setup to compare the current results with the data of Mat et al. [44]. This way, the inner tube radius, middle tube radius, outer tube radius, and length of the numerical model are considered 25.4 mm, 75 mm, 100 mm, and 200 mm, respectively. Also, RT82 is regarded as the PCM of the unit. The comparison between the PCM mean temperature during the melting procedure in the experimental investigation of Mat et al. and the present investigation [44] is provided in Fig. 5 (b). According to this figure, the results of the two studies show an excellent agreement. The maximum and average errors between the studies are 3.2 % and 2.1 %, respectively.

5. Numerical results

In this part, the thermal, electrical, and overall performances of the three hybrid units, namely ETC-PCM, ETC-PV-PCM, and ETC-PV-PCM integrated with metal foam are expressed, and the best unit from the energy viewpoint is detected. Additionally, the influence of some factors, including the PCM melting temperature, the mass fraction of nanoparticles, and fluid mass flow rate on the performance of the best unit is investigated. The following results of the simulation of the units are presented.

The amount of operating fluid outlet temperature, value of melted PCM, and PV layer temperature, in different units, are pictured in Fig. 5. As shown in this figure, the lowest and highest average outlet temperature belongs to the ETC-PV-PCM and ETC-PCM units, respectively. The operating fluid outlet temperature in the ETC-PCM unit has its highest value collated with the other units due to the absence of the solar cell layer. The PV module converts a portion of solar energy into electrical energy. Thus, lower thermal flux is transferred to the PCM and operating fluid. On the other hand, installing porous metal foam inside the tube of the ETC-PV-PCM unit improves the operating fluid outlet temperature, which is attributed to the enhancement in the transferred heat from the PCM to the stream. Regarding the conventional tube, the temperature of the operating fluid adjacent to the tube wall is remarkably higher than the temperature of the fluid at the center of the tube because of poor conduction characteristics of the operating fluid. However, the porous metal foam has a high thermal conductivity, reducing the temperature variation between the central and fluid layers attached to the tube. Therefore, by reducing the temperature of the adjacent layer, the ability of the operating fluid in thermal energy absorption from the PCM increases.

Nevertheless, the outlet temperature of the ETC-PV-PCM unit is higher than the operating fluid outlet temperature in the FETC-PV-PCM unit after 16:00, which is attributed to the transfer of liquid materials to the solid state. In the ETC-PV-PCM unit, the PCM stores higher thermal energy, which releases to the unit during low solar radiation periods. The results show that the average operating fluid final temperature for the PCM-based ETC, ETC-PV-PCM, and FETC-PV-PCM is 32.88 °C, 32.64 °C, and 32.70 °C, respectively.

Also, based on Fig. 5, installing copper foam inside the tube reduces the PV temperature. Indeed, by increasing the thermal quantity of the fluid, the unit's temperature reduces, including the PV layer. So, the unit

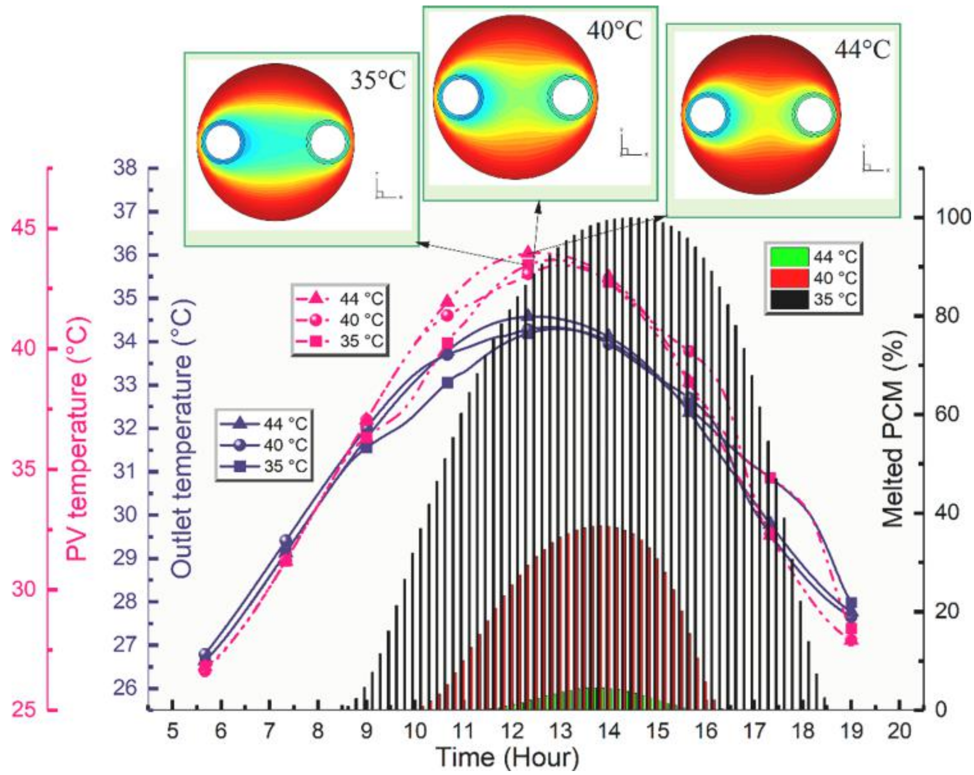

Fig. 10. The variation of melted PCM, outlet temperature, and PV layer temperature of FETC-PV-PCM unit at different PCM melting points.

will produce more electrical energy in the presence of metal foam inside the fluid channel. Moreover, a lower amount of solid PCM is transferred to the liquid state due to reducing the unit's temperature using metal foam. Achieved outcomes show that the maximum amount of melted PCM for the PCM-based ETC, ETC-PV-PCM, and FETC-PV-PCM units are 65 %, 57 %, and 37 %, respectively.

The thermal, electrical, and overall performance of the simulated units at the base case condition are depicted in Fig. 6 (a), (b), and (c), respectively. Moreover, the average performance of the units during the day is pictured in Fig. 6 (d). As depicted in Fig. 6 (a), the PCM-based ETC unit has the highest thermal output among the simulated units. However, integrating the unit with the PV module reduces unit thermal power, which is due to electricity production by the PV module. Combining the ETC-PCM unit with the PV module reduces the thermal power of the ETC unit from 33.89 W to 31.84 W.

Moreover, it is concluded that installing metal foam in the fluid channel causes an enhancement in unit thermal power, which can be attributed to the higher interaction between the water and the pipe. Based on the results, installing metal foam in the fluid channel of the ETC-PV-PCM unit improves the thermal power of the unit from 31.84 W to 32.29 W. Also, a slight increment in the unit electricity production is created by filling the fluid channel with porous foam (Fig. 6 (b)).

According to the numerical simulations, the FETC-PV-PCM and ETC-PCM hybrid units have the highest and lowest overall performance among the studied cases, respectively. The overall output power of the ETC-PCM, ETC-PV-PCM, and FETC-PV-PCM units are 33.89 W, 37.93 W, and 38.42 W, respectively. Thus, for the following simulations, the influence of various factors is examined only on the FETC-PV-PCM hybrid unit.

Fig. 7 shows the consequence of operating fluid flow level on the outlet temperature, amount of melted PCM, and PV layer temperature of the FETC-PV-PCM renewable unit. As can be seen, raising the mass flow rate from 3.6 L/h to 10.8 L/h reduces both outlet temperature and the operating fluid and PV layer temperature remarkably. According to the results, the maximum outlet temperature at the operating fluid flow levels of 3.599 L/h, 7.198 L/h, and 10.81 L/h are 42.4 °C, 36.4 °C, and 34.2 °C, accordingly.

Escalating the mass flow level of fluid reduced the PV layer temperature, and a reduction in the amount of melted PCM in the high mass flow rates can be concluded. The maximum temperature of the PV layer at the fluid mass levels of 3.6 L/h, 7.201 L/h, and 10.801 L/h are 48.58 °C, 43.47 °C, and 43.01 °C, respectively. As observed, in the unit with the water mass flow rate of 3.6 L/h, the PCM starts to melt at around 09:00. In comparison, PCM starts to melt around 10:00 for the unit with the water mass flow rate of 7.2 L/h and 10.8 L/h. The first part of the PCM that starts to melt is the materials adjacent to the upper area of the absorber layer, which is toward the sky.

Based on the results, boosting the flow level from 3.6 to 7.2 L/h has a higher impact on the temperature of the unit than the elevation of the flow level from 7.2 to 10.8 L/h. This phenomenon is attributed to the variation of PV layer temperature, amount of melted PCM, and outlet temperature versus the fluid flow level. However, reducing the operating fluid outlet temperature (by raising the fluid mass flow rate) does not lead to a decline in the thermal output power of the unit.

In Fig. 8 (a), the system net power at some operating fluid mass flow rates is depicted. According to this figure, rising the fluid flow level enhances the overall output of the unit. Increasing the mass flow level inside the fluid channel has a constructive influence on the unit's electrical and energy performance. The thermal outputs of the proposed unit at the fluid level of 10.8 L/h are 1.1 % and 4.5 % higher than that of the unit at working mass flow rates of 7.2 L/h and 3.6 L/h, respectively. Also, the mean power of the unit for the flow levels of 3.599 L/h, 7.201 L/h, and 10.799 L/h are 38.55 W, 39.75 W, and 40.13 W, accordingly. Elevating the fluid flow level enhances the quantity of transferred heat

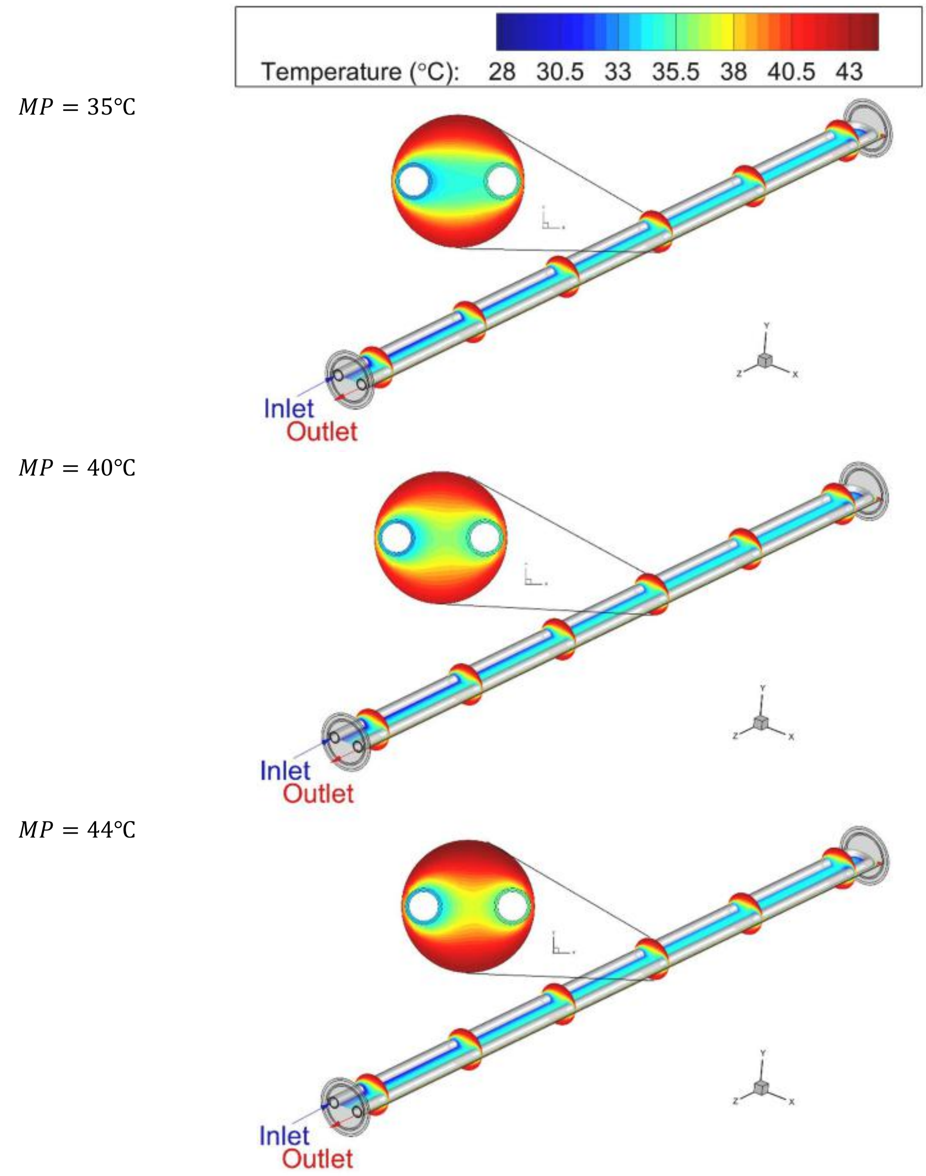

Fig. 11. Temperature distribution in the presented FETC-PV-PCM hybrid unit utilizing various melting points at noon.

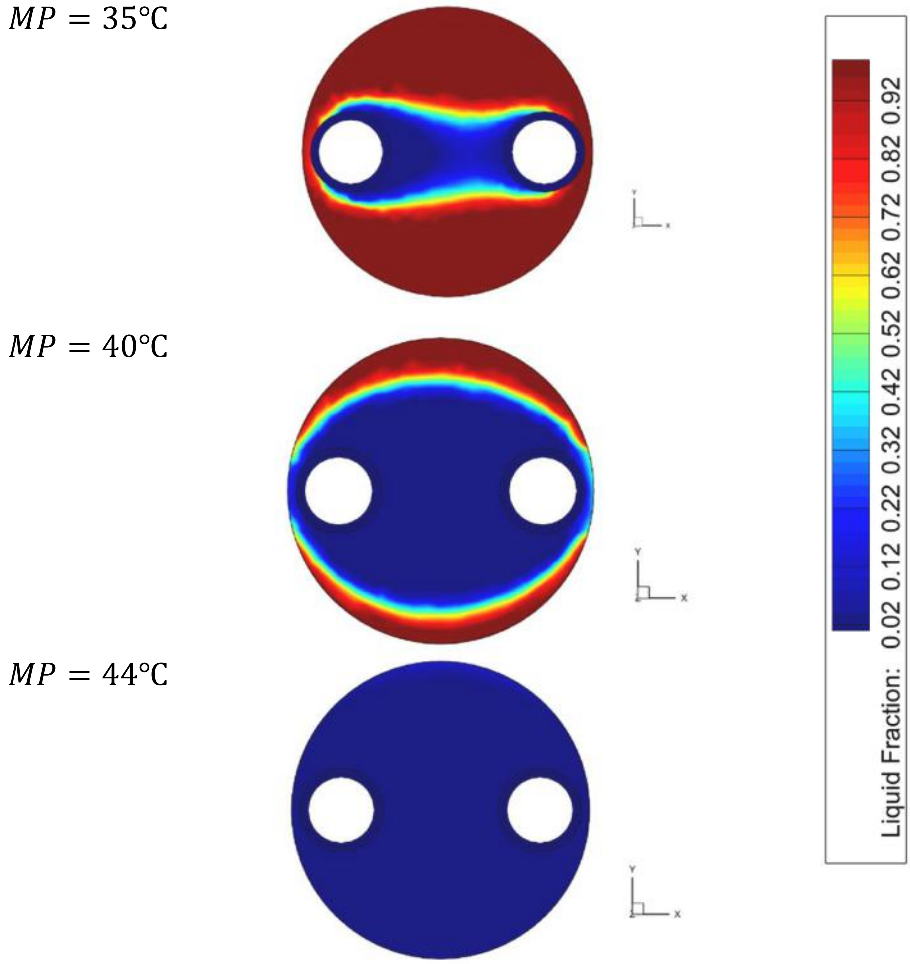

Fig. 12. PCM liquid fraction in the proposed FETC-PV-PCM hybrid unit using the material with various melting points at noon.

from the copper pipe to the unit due to increasing the convection heat transfer factor, which is due to raising the fluid velocity in the pipe. Lifting the flow level from 3.6 to 7.2 L/h remarkably increases the convective heat transfer coefficient, and further raising the mass flow rate is not considerably influential on the transmitted heat to the operating fluid.

Moreover, the thermal, electrical, and energy loss of the unit at the water flow level of 10.8 LPM is presented in Fig. 8 (b). This figure shows that the unit produces the highest electrical and thermal energy value at noontime. Also, the highest energy loss of the unit belongs to this time. According to this figure, the amount of lost energy before sunset is negative. During this period, the PCM releases the stored heat to the unit. Thus, before sunset, the overall output power of the unit is more than the received input solar energy by the unit. This figure shows that most of the accumulated energy in the PCM transfers from the PCM to the operating fluid at 16:00.

The impact of the PCM melting temperature on melted PCM, PV temperature, and outlet temperature of the FETC-PV-PCM hybrid unit at the flow level of 10.8 L/h are demonstrated in Fig. 9. As can be seen, the reduction in the PCM melting spot leads to declination and increment in the outlet temperature of the operating fluid before noon and sunset, respectively. Reducing the melting point from 44 °C to 35 °C diminishes the fluid final temperature from 34.54 °C to 34.05 °C at noontime. At the same time, this variation in the melting spot of the PCM enhances the fluid final temperature from 31.84 °C to 32.12 °C at 16:00.

Acquiring the PCM temperature to its melting temperature will store a huge part of the thermal energy in this component. Thus, fewer energy shifts from the mentioned unit to the operating fluid. By reducing the DNI in the evening and declination in the PCM temperature, the melted PCM transfer from the liquid to the solid state. As a result, the stored energy in the PCM transfers to the fluid, increasing the outlet temperature.

As depicted in Fig. 9, during the PCM melting procure, the temperature of the PV layer reduces, which causes higher electricity generation by the proposed unit. However, due to the heat transmission process from the PCM to the unit in the evening, the PV layer temperature is more than that of the PCM-based unit at high melting temperatures.

The temperature distribution of the proposed FETC-PV-PCM hybrid unit using PCM with the various melting temperatures at noon is illustrated in Fig. 10. Considering this plot, increasing the PCM melting temperature from 35 °C to 40 °C reduces the PV surface temperature. Indeed, a massive part of the PCM with the melting spot of 35 °C is thawed until noon. Thus, this type of material has not significant cooling effect in the noon. Also, the unit utilizing PCM with the melting temperature of 44 °C has the highest surface temperature among the studied cases.

Moreover, the PCM liquid fraction at different melting points in the noon is depicted in Fig. 11. According to Fig. 11, an increase in PCM melting temperature reduces the quantity of melted PCM. As presented, the PCM starts to melt initially in the lower and upper sections adjacent to the absorber layer. Also, the last area where the PCM will melt is near the fluid channel due to the extremely low temperature. Additionally, in the proposed FETC-PV-PCM hybrid unit, using PCM with the melting temperature of 44 °C, just a small fraction of the PCM got melted, which

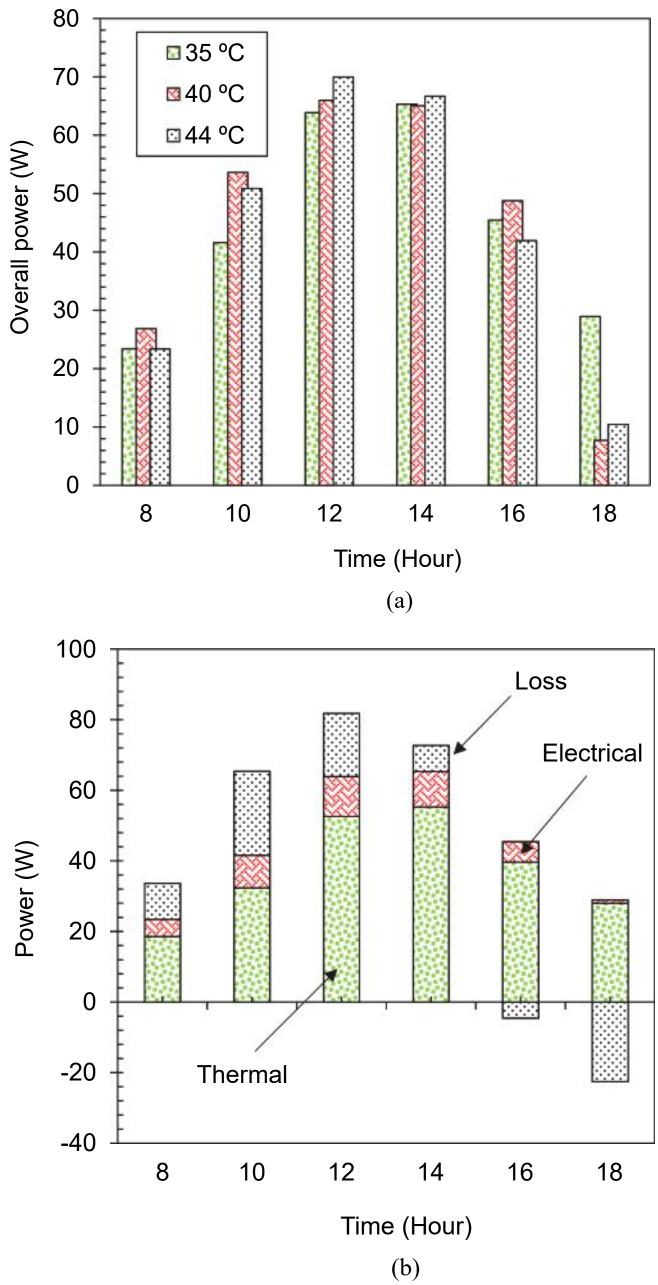

Fig. 13. The overall performance of different units at different PCM melting points and (b) the detailed performance of the unit by utilizing PCM with the melting spot of 35 °C.

can be attributed to the high melting temperature of the PCM.

The overall output of the proposed FETC-PV-PCM hybrid unit at various melting temperatures is reported in Fig. 12 (a). As shown in this figure, the thermal output of the FETC-PV-PCM generation unit using PCM with the melting point of 35 °C, 40 °C, and 44 °C is 52.60 W, 54.22 W, and 58.74 W, accordingly. The electrical power of the unit is calculated to be 11.27 W, 11.76 W, and 11.23 W by utilizing PCM with the melting spot of 35 °C, 40 °C, and 44 °C, respectively. Based on the results, the unit utilizing PCM with the melting temperature of 44 °C has the highest overall performance in the noontime compared to the other units. At this time, the FETC-PV-PCM unit using PCM with a melting spot of 35.1 °C and 40 °C, a considerable section of thermal quantity is accumulated in the PCM through the melting process. While in the unit using PCM with the melting temperature of 44 °C, most heat transfers to the fluid. Thus, the outlet temperature of the heat transfer fluid increases by raising the melting point of the unit. However, this phenomenon negatively influences the electrical production of the unit. In the unit using PCM with high melting points, the system operates at high temperatures leading to a decrease in the output of the cell, which is highly dependent on the temperature.

On the other hand, in the afternoon, the unit by PCM with poor melting points has higher overall performance due to the heat transmit phenomenon from the PCM layer to the fluid through solidification procure.

In Fig. 12 (b), the variation of detailed performance of the proposed FETC-PV-PCM hybrid unit with time at the melting temperature of 35 °C is depicted. By comparing this figure with Fig. 8 (b), it can be seen that the highest thermal power production by the unit transferred from noon to 14:00. However, most of the electricity is still produced by the unit at noon. Also, it can be concluded that utilizing PCM with a lower melting temperature will transfer most of the heat from the PCM layer to the unit at near sunset. Because of the low melting temperature of PCM, the melted materials remain liquid until a considerable reduction occurs in the solar radiation, which happens near sunset. At this time, the unit temperature reaches the PCM solidification temperature, leading to heat transmission from the PCM to the unit at a constant temperature. Moreover, the reduction in the PCM melting spot increases the heat loss of the unit until noon; while, it enhances the heat transition rate between the unit and PCM before sunset.

Fig. 13 presents the quantity of melted PCM, final temperature of the fluid, and PV layer temperature of the FETC-PV-PCM unit with various nanoparticle mass fractions. As presented, MWCNT nanoparticle dispersion in the water rises the operating fluid outlet temperature and the PV layer temperature. Adding the nanoparticles to the operating fluid of the mentioned unit raises the thermal properties of the mixture, which raises the heat transition toward the fluid. This enhancement leads to an increment in the outlet temperature of the fluid and a decline in the temperature of the PV cells. For instance, at noontime, the outlet temperature of the unit with nanoparticles mass fraction of 2 % wt. and 4 % wt. are calculated to be 0.57 % and 0.86 % higher than that of the unit with pure water. Furthermore, at the same time of the day, the temperature of MWCNT/water (2 % wt.), MWCNT/water (4 % wt.), and the PV layer in the water, based units are 43.01 °C, 42.81 °C, and 43.13 °C, respectively.

Furthermore, the overall efficiency of the proposed FETC-PV-PCM hybrid unit with different operating fluids of MWCNT/water (2 % wt.), pure water, and MWCNT/water (4 % wt.) are presented in Fig. 14 (a). As depicted, the unit with operating fluids of pure water and MWCNT/water (4 % wt.) has the lowest and highest overall performance among the units. The unit with operating fluids of pure water, MWCNT/water (2 % wt.), and MWCNT/water (4 % wt.) have an average overall energy output of 40.0 W, 41.0 W, and 41.4 W, respectively (see Fig. 15).

The detailed performance of the FETC-PV-PCM unit by using MWCNT/water (4 % wt.) as the operating fluid is demonstrated in Fig. 14 (b). By comparing this figure with Fig. 12 (b), it can be revealed that nanoparticle scattering in the base liquid enhances the electrical and thermal outputs of the unit. Also, considering nanofluid as the operating fluid reduces the heat loss of the proposed unit.

According to the performed simulations, the FETC-PV-PCM unit at the fluid mass flow rate of 10.8 L/h, RT-44 PCM, and MWCNT/water (4 % wt.) has the highest overall output.

6. Conclusion

In this numerical assessment, the operation of three different units, including integration of Phase Change Materials with an evacuated tube solar collector (ETC-PCM), an evacuated tube solar collector merged with Photovoltaic (PV) cell and PCM (ETC-PV-PCM), and an evacuated tube solar collector combined with metal foam, PCM, and PV cell (FETC-PV-PCM) is studied. Initially, the performance of these units is

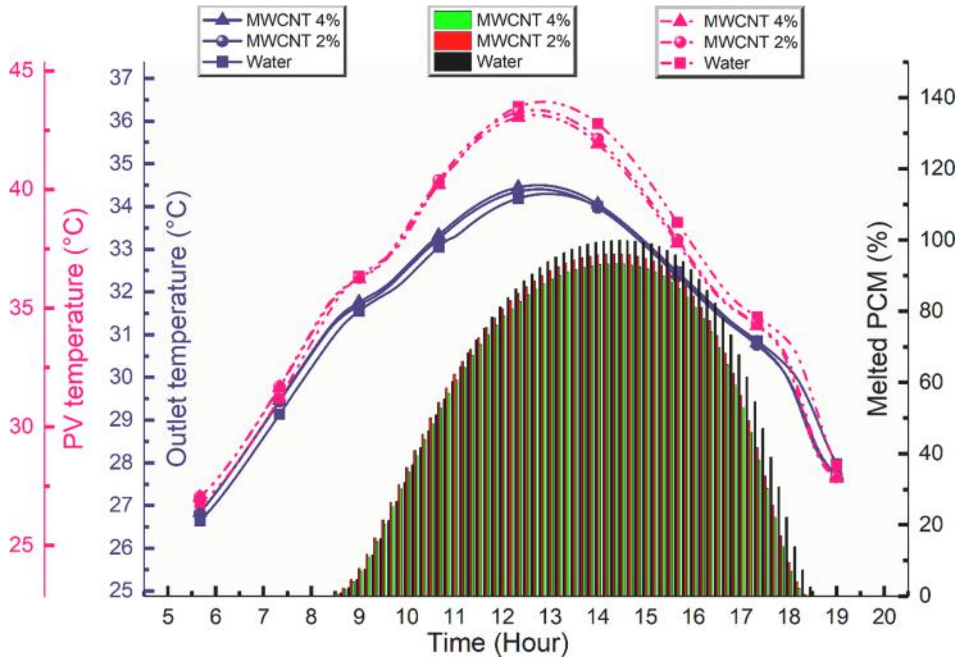

Fig. 14. The melted PCM, final temperature, and PV layer temperature of FETC-PV-PCM unit at different mass fractions of nanoparticles.

scrutinized under the transient weather at the base case condition. Henceforth, by comparing the unit's overall energy performance, the unit with the highest performance is chosen for further investigation. In this step, the unit is simulated under transient weather conditions by variation of parameters of the unit such as fluid flow level, the PCM melting spot, and MWCNT mass fraction. Finally, the best unit with the most proper working conditions is presented. The most remarkable findings of this study are listed as:

- The overall efficiency of the ETC-PV-PCM, ETC-PCM, and FETC-PV-PCM units are 37.93 W, 33.89 W, and 38.42 W, respectively. Thus, the FETC-PV-PCM hybrid unit has the greatest efficiency compared to the investigated cases.
- Increasing the fluid flow level enhances the thermal and electrical power of the FETC-PV-PCM unit. By raising the fluid flow level from 3.8 L/h to 10.8 L/h, the mean thermal power of the unit increases from 32.25 W to 33.71 W. Furthermore, by the same enhancement in the flow level, the average electrical output power of the unit improves from 6.30 W to 6.42 W.
- Reduction in the PCM melting temperature leads to declination in both the PV layer temperature and outlet temperature of the operating fluid in the noontime due to the heat absorption in this material during phase change procure from solid-state to liquid-state.
- Reduction in the PCM melting point has a favorable effect on the thermal and electrical output power of the FETC-PV-PCM unit. Raising the PCM melting spot from 44 °C to 35 °C elevates the overall performance of mentioned FETC-PV-PCM hybrid unit by 0.4 %.
- Raising the MWCNT mass fraction in the base fluid enhances the thermal properties, improving the overall performance of the unit. The overall performance of the MWCNT/water (4 % wt.) based FETC-PV-PCM unit is 3.37 % greater than that of the water-based FETC-PV-PCM generation unit.

The present study results show that the FETC-PV-PCM coupled unit at the fluid flow level of 10.8 L/h and implementing PCM with the melting point of 35 °C has the highest energy performance among the studied units. Moreover, the best operating fluid of the unit accounted for MWCNT/water (4 % wt.). However, some ideas can still attract researchers' attention to propose an ETC unit with higher performance. The suggested topics are:

- Adding fins inside the PCM media improves the heat transition rate between the absorber layers as well as the PCM and the operating fluid.
- Evaluating the effect of variation in the value of porosity, permeability, and foam material on the outputs of the FETC-PV-PCM unit.
- Adding metal nanoparticles in the PCM to boost the heat conduction coefficient of the mixture for enhancing the thermal conductivity through the generation unit.
- Investigation of the effect of the installation of metal foam in the PCM on the operation of the ETC-PV-PCM coupled unit.

CRediT authorship contribution statement

Xingxing Yang: Resources, Formal analysis, Investigation, Supervision. **Qing Lin:** Writing – review & editing, Methodology, Formal analysis, Data curation. **Pavitra Singh:** Methodology, Writing – original draft, Investigation. **Fahid Riaz:** Methodology, Writing – original draft, Investigation. **Manoj Kumar Agrawal:** Writing – review & editing, Methodology, Formal analysis, Data curation. **Theyab R. Alsenani:** Methodology, Formal analysis, Data curation, Investigation, Writing – review & editing, Resources. **Guangqiang Li Xia:** Writing – review & editing, Formal analysis, Resources. **Mostafa A.H. Abdelmohimen:** Writing – review & editing, Methodology, Formal analysis, Data curation.

Declaration of Competing Interest

The authors declare that they have no known competing financial interests or personal relationships that could have appeared to influence the work reported in this paper.

Data availability

No data was used for the research described in the article.

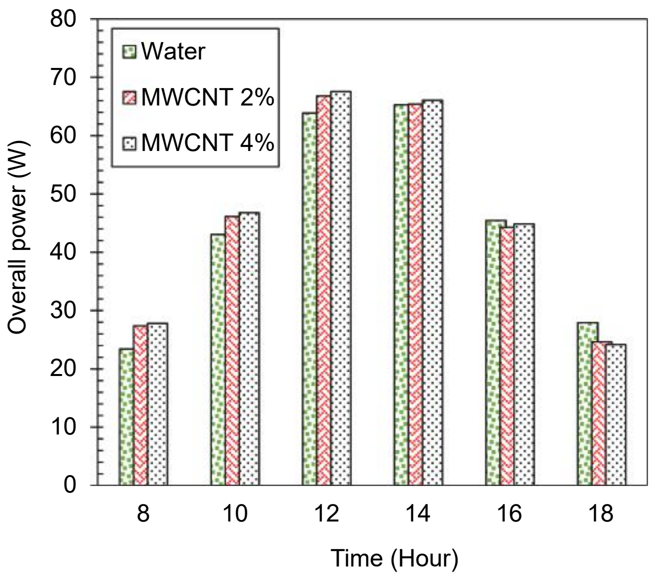

(a)

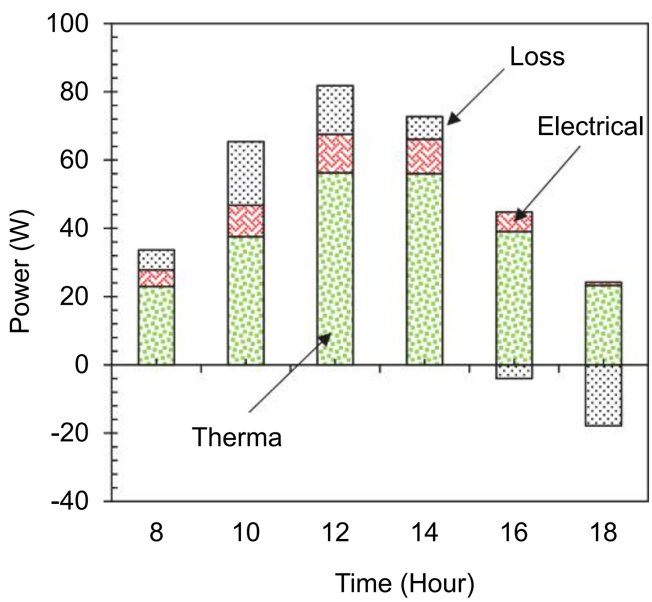

(b)

Fig. 15. The overall performance of different units at various nanoparticle mass fractions and (b) the detailed performance of the proposed unit with MWCNT/water (4 % wt.).

Acknowledgment

The authors extend their appreciation to the Deanship of Scientific Research at King Khalid University for funding this work through Large Groups (RGP.2/94/43).

This work was financially supported by the National Natural Science Foundation of China (No. 12164006).All authors discussed the results and commented on the manuscript.

This study is supported via funding from Prince Sattam bin Abdulaziz University project number (PSAU/2023/R/1444).

References

[1] M. Ghalambaz, J. Zhang, Conjugate solid-liquid phase change heat transfer in heatsink filled with phase change material-metal foam, Int. J. Heat Mass Transf. 146 (2020), 118832.

[2] M. Carmona, A. Palacio, J.D. García, Experimental evaluation of a hybrid photovoltaic and thermal solar energy collector with integrated phase change material (PVT-PCM) in comparison with a traditional photovoltaic (PV) module, Renew. Energy (2021).

[3] C. Ho, Y.-C. Liu, M. Ghalambaz, W.-M. Yan, Forced convection heat transfer of Nano-Encapsulated Phase Change Material (NEPCM) suspension in a mini-channel heatsink, Int. J. Heat Mass Transf. 155 (2020), 119858.

[4] G. Asefi, T. Ma, R. Wang, Parametric investigation of photovoltaic-thermal systems integrated with porous phase change material, Appl. Therm. Eng. 201 (2022), 117727.

[5] M. Alizadeh, M.H. Shahavi, D.D. Ganji, Performance enhancement of nano PCM solidification in a hexagonal storage unit with innovative fin shapes dealing with time-dependent boundary conditions, Energy Rep. 8 (2022) 8200–8214.

[6] A. NematpourKeshteli, M. Iasiello, G. Langella, N. Bianco, Enhancing PCMs thermal conductivity: a comparison among porous metal foams, nanoparticles and finned surfaces in triplex tube heat exchangers, Appl. Therm. Eng. 212 (2022), 118623.

[7] M. Ghalambaz, S.M.H. Zadeh, S. Mehryan, I. Pop, D. Wen, Analysis of melting behavior of PCMs in a cavity subject to a non-uniform magnetic field using a moving grid technique, App. Math. Model. 77 (2020) 1936–1953.

[8] A. Papadimitratos, S. Sobhansarbandi, V. Pozdin, A. Zakhidov, F. Hassanipour, Evacuated tube solar collectors integrated with phase change materials, Sol. Energy 129 (2016) 10–19.

[9] M.A. Essa, N.H. Mostafa, M.M. Ibrahim, An experimental investigation of the phase change process effects on the system performance for the evacuated tube solar collectors integrated with PCMs, Energ. Conver. Manage. 177 (2018) 1–10.

[10] K. Chopra, V. Tyagi, A.K. Pathak, A. Pandey, A. Sari, Experimental performance evaluation of a novel designed phase change material integrated manifold heat pipe evacuated tube solar collector system, Energ. Conver. Manage. 198 (2019), 111896.

[11] M.H. Abokersh, M. El-Morsi, O. Sharaf, W. Abdelrahman, An experimental evaluation of direct flow evacuated tube solar collector integrated with phase change material, Energy 139 (2017) 1111–1125.

[12] K. Chopra, A.K. Pathak, V. Tyagi, A. Pandey, S. Anand, A. Sari, Thermal performance of phase change material integrated heat pipe evacuated tube solar collector system: an experimental assessment, Energ. Conver. Manage. 203 (2020), 112205.

[13] H. Olfian, S.S.M. Ajarostaghi, M. Farhadi, A. Ramiar, Melting and solidification processes of phase change material in evacuated tube solar collector with U-shaped spirally corrugated tube, Appl. Therm. Eng. 182 (2021), 116149.

[14] M.A. Essa, I.Y. Rofaiel, M.A. Ahmed, Experimental and theoretical analysis for the performance of evacuated tube collector integrated with helical finned heat pipes using PCM energy storage, Energy 206 (2020), 118166.

[15] L. Feng, J. Liu, H. Lu, Y. Chen, S. Wu, A parametric study on the efficiency of a solar evacuated tube collector using phase change materials: a transient simulation, Renew. Energy 199 (2022) 745–758.

[16] S. Aberoumand, S. Ghamari, B. Shabani, Energy and exergy analysis of a photovoltaic thermal (PV/T) system using nanofluids: an experimental study, Sol. Energy 165 (2018) 167–177.

[17] S.M. Parsa, A. Yazdani, H. Aberoumand, Y. Farhadi, A. Ansari, S. Aberoumand, N. Karimi, M. Afrand, G. Cheraghian, H.M. Ali, A critical analysis on the energy and exergy performance of photovoltaic/thermal (PV/T) system: the role of nanofluids stability and synthesizing method, Sustainable Energy Technol. Assess. 51 (2022), 101887.

[18] G. Sadeghi, S. Nazari, M. Ameri, F. Shama, Energy and exergy evaluation of the evacuated tube solar collector using Cu2O/water nanofluid utilizing ANN methods, Sustainable Energy Technol. Assess. 37 (2020), 100578.

[19] I. Mahbubul, M.M.A. Khan, N.I. Ibrahim, H.M. Ali, F.A. Al-Sulaiman, R. Saidur, Carbon nanotube nanofluid in enhancing the efficiency of evacuated tube solar collector, Renew. Energy 121 (2018) 36–44.

[20] Z. Said, A.A. Hachicha, S. Aberoumand, B.A. Yousef, E.T. Sayed, E. Bellos, Recent advances on nanofluids for low to medium temperature solar collectors: energy, exergy, economic analysis and environmental impact, Prog. Energy Combust. Sci. 84 (2021), 100898.

[21] H. Kaya, M. Alkasem, K. Arslan, Effect of nanoparticle shape of Al2O3/Pure Water nanofluid on evacuated U-Tube solar collector efficiency, Renew. Energy 162 (2020) 267–284.

[22] S.M.S. Hosseini, M.S. Dehaj, Assessment of TiO2 water-based nanofluids with two distinct morphologies in a U type evacuated tube solar collector, Appl. Therm. Eng. 182 (2021), 116086.

[23] A. Kazemian, A. Salari, T. Ma, H. Lu, Application of hybrid nanofluids in a novel combined photovoltaic/thermal and solar collector system, Sol. Energy 239 (2022) 102–116.

[24] M. Hosseinzadeh, A. Salari, M. Sardarabadi, M. Passandideh-Fard, Optimization and parametric analysis of a nanofluid based photovoltaic thermal system: 3D numerical model with experimental validation, Energ. Conver. Manage. 160 (2018) 93–108.

[25] M. Iasiello, M. Mameli, S. Filippeschi, N. Bianco, Simulations of paraffine melting inside metal foams at different gravity levels with preliminary experimental validation, in: Journal of Physics: Conference Series, Vol. 1599, IOP Publishing, 2020, pp. 012008.

[26] K. Venkateshwar, S. Tasnim, H. Simha, S. Mahmud, Influence of metal foam morphology on phase change process under temporal thermal load, Appl. Therm. Eng. 180 (2020), 115874.

[27] A. Arshad, M. Jabbal, H. Faraji, P. Talebizadehsardari, M.A. Bashir, Y. Yan, Thermal performance of a phase change material-based heat sink in presence of

nanoparticles and metal-foam to enhance cooling performance of electronics, J. Storage Mater. 48 (2022), 103882.
[28] H. Pierrick, M. Christophe, G. Leon, D. Patrick, Dynamic numerical model of a high efficiency PV–T collector integrated into a domestic hot water system, Sol. Energy 111 (2015) 68–81.
[29] J.J. Michael, I. Selvarasan, R. Goic, Fabrication, experimental study and testing of a novel photovoltaic module for photovoltaic thermal applications, Renew. Energy 90 (2016) 95–104.
[30] A. Salari, A. Kazemian, T. Ma, A. Hakkaki-Fard, J. Peng, Nanofluid based photovoltaic thermal systems integrated with phase change materials: numerical simulation and thermodynamic analysis, Energ. Conver. Manage. 205 (2020), 112384.
[31] B.C. Pak, Y.I. Cho, Hydrodynamic and heat transfer study of dispersed fluids with submicron metallic oxide particles, Exp. Heat Transf. Int. J. 11 (1998) 151–170.
[32] M. Corcione, Empirical correlating equations for predicting the effective thermal conductivity and dynamic viscosity of nanofluids, Energ. Conver. Manage. 52 (2011) 789–793.
[33] Y. Xuan, Q. Li, W. Hu, Aggregation structure and thermal conductivity of nanofluids, AIChE J. 49 (2003) 1038–1043.
[34] A. Fluent, Ansys fluent theory guide, Ansys Inc., USA, 15317 (2011) 724–746.
[35] J.M. Mahdi, R.P. Singh, H.M.T. Al-Najjar, S. Singh, E.C. Nsofor, Efficient thermal management of the photovoltaic/phase change material system with innovative exterior metal-foam layer, Sol. Energy 216 (2021) 411–427.
[36] A. Salari, M. Ashouri, A. Hakkaki-Fard, On the performance of inclined rooftop solar chimney integrated with photovoltaic module and phase change material: a numerical study, Sol. Energy 211 (2020) 1159–1169.
[37] H. Pourrahmani, M. Moghimi, M. Siavashi, M. Shirbani, Sensitivity analysis and performance evaluation of the PEMFC using wave-like porous ribs, Appl. Therm. Eng. 150 (2019) 433–444.
[38] N. Variji, M. Siavashi, M. Tahmasbi, M. Bidabadi, Analysis of the effects of porous media parameters and inclination angle on the thermal storage and efficiency improvement of a photovoltaic-phase change material system, J. Storage Mater. 50 (2022), 104690.
[39] S. Lugo, O. García-Valladares, R. Best, J. Hernández, F. Hernández, Numerical simulation and experimental validation of an evacuated solar collector heating system with gas boiler backup for industrial process heating in warm climates, Renew. Energy 139 (2019) 1120–1132.
[40] D. Evans, Simplified method for predicting photovoltaic array output, Sol. Energy 27 (1981) 555–560.
[41] X. Ju, M.M. Abd El-Samie, C. Xu, H. Yu, X. Pan, Y. Yang, A fully coupled numerical simulation of a hybrid concentrated photovoltaic/thermal system that employs a therminol VP-1 based nanofluid as a spectral beam filter, Appl. Energy 264 (2020), 114701.
[42] S. Mullick, S. Nanda, An improved technique for computing the heat loss factor of a tubular absorber, Sol. Energy 42 (1989) 1–7.
[43] W.C. Swinbank, Long-wave radiation from clear skies, Q. J. R. Meteorolog. Soc. 89 (1963) 339–348.
[44] S. Mat, A.A. Al-Abidi, K. Sopian, M.Y. Sulaiman, A.T. Mohammad, Enhance heat transfer for PCM melting in triplex tube with internal–external fins, Energ. Conver. Manage. 74 (2013) 223–236.